

A Statistical Dynamical Model to Predict Extreme Events and Anomalous Features in Shallow Water Waves with Abrupt Depth Change

Andrew J. Majda^{a,1}, M. N. J. Moore^b, and Di Qi^{a,1}

^aDepartment of Mathematics and Center for Atmosphere and Ocean Science, Courant Institute of Mathematical Sciences, New York University, New York, NY 10012;

^bDepartment of Mathematics and Geophysical Fluid Dynamics Institute, Florida State University, Tallahassee, FL

This manuscript was compiled on November 25, 2018

Understanding and predicting extreme events and their anomalous statistics in complex nonlinear systems is a grand challenge in climate, material, and neuroscience, as well as for engineering design. Recent controlled laboratory experiments in weakly turbulent shallow water with abrupt depth change (ADC) exhibit a remarkable transition from nearly Gaussian statistics in incoming wave trains before the ADC to outgoing waves trains after the ADC with extreme anomalous statistics with large positive skewness of the surface height. Here we develop a statistical dynamical model to explain and quantitatively predict the above anomalous statistical behavior as experimental control parameters are varied. The first step is to use incoming and outgoing truncated Korteweg-de Vries (TKdV) equations matched in time at the ADC. The TKdV equation is a Hamiltonian system which induces incoming and outgoing statistical Gibbs invariant measures which are statistically matched at the ADC. The statistical matching of the known nearly Gaussian incoming Gibbs state at the ADC completely determines the predicted anomalous outgoing Gibbs state, which can be calculated by a simple sampling algorithm, verified by direct numerical simulations, and successfully captures key features of the experiment. There is even an analytic formula for the anomalous outgoing skewness. The strategy here should be useful for predicting extreme anomalous statistical behavior in other dispersive media in different settings.

extreme anomalous event | statistical TKdV model | matching Gibbs measures | surface wave displacement and slope

Understanding and predicting extreme events and their anomalous statistics in complex nonlinear systems is a grand challenge in climate, material and neuroscience as well as for engineering design. This is a very active contemporary topic in applied mathematics with qualitative and quantitative models (1–7) and novel numerical algorithms which overcome the curse of dimensionality for extreme event prediction in large complex systems (2, 8–11). The occurrence of Rogue waves as extreme events within different physical settings of deep water (12–16) and shallow water (17–19) is an important practical topic.

Recent laboratory experiments in weakly turbulent shallow water reveal a remarkable transition from Gaussian to anomalous behavior as surface waves cross an abrupt depth change (ADC). A normally-distributed incoming wave train, upstream of the ADC, transitions to a highly non-Gaussian outgoing wave train, downstream of the ADC, that exhibits large positive skewness of the surface height and more frequent extreme events (20). Here we develop a statistical dynamical model to explain and quantitatively predict this anomalous behavior as experimental control parameters are varied. The first step is to use incoming and outgoing truncated Korteweg-de Vries

(TKdV) equations matched in time at the ADC. The TKdV equation is a Hamiltonian system which induces incoming and outgoing statistical Gibbs invariant measures which are statistically matched at the ADC. The statistical matching of the known nearly Gaussian incoming Gibbs state at the ADC completely determines the predicted anomalous outgoing Gibbs state, which can be calculated by a simple MCMC algorithm, verified by direct numerical simulations, and successfully captures key features of the experiment. There is even an analytic formula for the anomalous outgoing skewness. The strategy here should be useful for predicting extreme anomalous statistical behavior in other dispersive media in different settings.

If you like, we could cite papers on ‘Optical rogue waves’ and/or rogue waves in microwave systems here.

1. Experiments showing anomalous wave statistics induced by an abrupt depth change

Controlled laboratory experiments were carried out in (20) to examine the statistical behavior of surface waves crossing an ADC. In these experiments, nearly unidirectional waves are generated by a paddle wheel and propagate through a long, narrow wave tank. Midway through, the waves encounter a

Significance Statement

Understanding and predicting extreme events and their anomalous statistics in complex nonlinear systems is a grand challenge in applied sciences as well as for engineering design. Recent controlled laboratory experiments in weakly turbulent shallow water with abrupt depth change exhibit a remarkable transition from nearly Gaussian statistics to extreme anomalous statistics with large positive skewness of the surface height. We develop a statistical dynamical model to explain and quantitatively predict the anomalous statistical behavior. The incoming and outgoing waves are modeled by the truncated Korteweg-de Vries equations statistically matched at the depth change. The statistical matching of the known nearly Gaussian incoming Gibbs state completely determines the predicted anomalous outgoing Gibbs state, and successfully captures key features of the experiment.

A.J.M. designed the research. A.J.M., M.N.J.M., and D.Q. performed the research. A.J.M., M.N.J.M., and D.Q. wrote the paper.

The authors declare no conflict of interest.

¹To whom correspondence should be addressed. E-mail: qidi@cims.nyu.edu, jonjon@cims.nyu.edu

125 step in the bottom topography, and thus abruptly transition
 126 from one depth to another. The paddle wheel is forced with
 127 angle
 128
 129 $\theta(t) = \theta_0 + \Delta\theta \sum_{n=1}^N a_n \cos(\omega_n t + \delta_n)$, $E \sim (\Delta\theta)^2 \sum_n a_n^2 \omega_n^2$.
 130
 131
 132 where the weights a_n are Gaussian in spectral space. The
 133 peak frequency ω_p gives rise to a characteristic wavelength λ_c
 134 of water waves, which can be estimated using the dispersion
 135 relation. Above, the total energy E in the system is determined
 136 by the angle amplitude $\Delta\theta$. Optical measurements of the free
 137 surface reveal a number of surprising statistical features:
 138
 139 • Distinct statistics are found between the incoming and
 140 outgoing wave disturbances: incoming waves display near-
 141 Gaussian statistics, while outgoing waves skew strongly
 142 towards positive displacement.
 143
 144 • The degree of non-Gaussianity present in the outgoing
 145 wave field depends on the total energy of the system: larger
 146 driving amplitudes $\Delta\theta$ generate stronger skewness in the
 147 surface displacement PDFs.
 148
 149 • The waves also show different characteristic peak wave-
 150 lengths in incoming and outgoing flows.
 151

I am not sure we need to include this last item. It is not really an experimental observation, simply a calculation that can be done using the dispersion relation and the values of the two depths. Could we simply take this last item out? Would you prefer to replace it with another observation? I could easily come up with one. Perhaps a comment on the decay rate of the power spectra.

2. Surface wave turbulence modeled by truncated KdV equation with depth dependence

The surface wave turbulence is modeled by a one-dimensional deterministic dynamical model.

This first sentence seems awkward to me.

The Korteweg-de Vries (KdV) equation (21) is a leading-order approximation of the surface waves that are determined by the balance of nonlinear and dispersive effects in an appropriate far-field limit. Here, the KdV equation is truncated in the first Λ modes (with $J = 2\Lambda + 1$ grid points) to generate weakly turbulent dynamics. The surface displacement is described by the state variable $u_\Lambda^\pm(x, t)$ with superscript ‘-’ for the incoming waves and ‘+’ for the outgoing waves. The Galerkin truncated variable $u_\Lambda = \sum_{1 \leq |k| \leq \Lambda} \hat{u}_k(t) e^{ikx}$ is normalized with zero mean $\hat{u}_0 = 0$ and unit energy $2\pi \sum_{k=1}^\Lambda |\hat{u}_k|^2 = 1$, which are conserved quantities, and $u_\Lambda \equiv \mathcal{P}_\Lambda u$ denotes the subspace projection. The evolution of u_Λ^\pm is governed by the truncated KdV equation with depth change D_\pm

$$\frac{\partial u_\Lambda^\pm}{\partial t} + \frac{D_\pm^{-3/2}}{2} E_0^{1/2} L_0^{-3/2} \frac{\partial}{\partial x} \mathcal{P}_\Lambda (u_\Lambda^\pm)^2 + D_\pm^{1/2} L_0^{-3} \frac{\partial^3 u_\Lambda^\pm}{\partial x^3} = 0, \quad [1]$$

on the normalized periodic domain $x \in [-\pi, \pi]$. The conserved Hamiltonian can be decomposed into a cubic and a quadratic term

$$\mathcal{H}_\Lambda^\pm = D_\pm^{-3/2} E_0^{1/2} L_0^{-3/2} H_3(u_\Lambda^\pm) - D_\pm^{1/2} L_0^{-3} H_2(u_\Lambda^\pm),$$

$$H_3(u) = \frac{1}{6} \int_{-\pi}^{\pi} u^3 dx, \quad H_2(u) = \frac{1}{2} \int_{-\pi}^{\pi} \left(\frac{\partial u}{\partial x} \right)^2 dx.$$

Equation [1] is non-dimensionalized in the periodic domain. The depth is assumed to be unit $D_- = 1$ before the ADC and becomes $D_+ < 1$ after the ADC. We introduce parameters (E_0, L_0, Λ) based on the following assumptions:

- The wavenumber truncation Λ is fixed in a moderate value for generating weakly turbulent dynamics;
- The state variable u_Λ^\pm is normalized with zero mean and unit energy, $\mathcal{M}(u_\Lambda) = 0, \mathcal{E}(u_\Lambda) = 1$, which are conserved during evolution. Meanwhile, E_0 characterizes the total energy injected into the system based on the paddle amplitude $(\Delta\theta)^2$;
- The length scale of the system is denoted L_0 . The value is chosen so that the resolved scale $\Delta x = 2\pi L_0/J$ is comparable to the characteristic wave length λ_c in the experiments.

Some intuition for how Eq. (1) produces different dynamics on either side of the ADC can be gained by considering the balance of the cubic and quadratic terms in the Hamiltonian \mathcal{H}_Λ^\pm . The depth change, $D_+ < 1$, increases the weight of H_3 and decreases that of H_2 , thus promoting the effects of nonlinearity and reducing dispersion. Since $\frac{\partial u}{\partial x}$ is the slope of the wave height, $H_2(u)$ measures the wave slope energy.

A *deterministic matching condition* is applied to the surface displacement u_Λ^\pm to link the incoming and outgoing wave trains. Assuming the abrupt depth change is met at $t = T_{\text{ADC}}$, the matching condition is given by

$$u_\Lambda^-(x, t)|_{t=T_{\text{ADC}}^-} = u_\Lambda^+(x, t)|_{t=T_{\text{ADC}}^+},$$

Equation [1] is not designed to capture the short scale changes in rapid time. Rather, since we are interested in modeling statistics before and after the depth change, we will examine the long-time dynamics of large-scale structures.

I modified the last sentence above. Feel free to revert to your original sentence if you do not like mine.

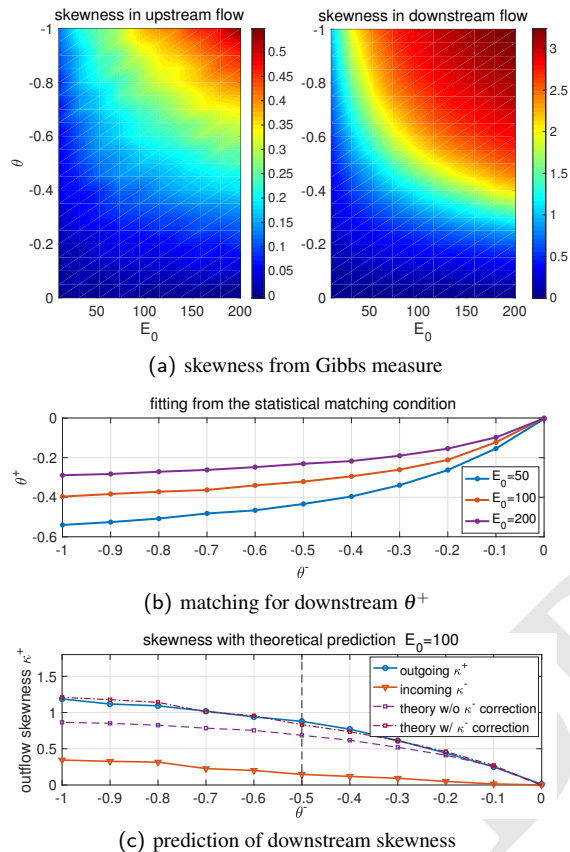
Interpreting experimental parameters in the dynamical model. The model parameters (E_0, L_0, Λ) in [1] can be directly linked to the basic scales from the physical problem. The important characterizing parameters measured from the experiments include: $\epsilon = \frac{a}{H_0}$ the wave amplitude a to water depth H_0 ratio; $\delta = \frac{H_0}{\lambda_c}$ the water depth to wavelength scale λ_c ratio; and $D_0 = \frac{d}{H_0}$ the normalized wave depth ratio with incoming flow depth $d = H_0$ to the outgoing flow depth $d < H_0$. The interpretations and reference values of these model parameters are based on the experimental setup (20). By comparing the characteristic physical scales, the normalized TKdV equation [1] can be linked directly with the measured non-dimensional quantities by

$$L_0 = 6^{\frac{1}{3}} \left(M \epsilon^{\frac{1}{2}} \delta^{-1} \right), \quad E_0 = \frac{27}{2} \gamma^{-2} \left(M \epsilon^{\frac{1}{2}} \delta^{-1} \right), \quad [2]$$

where M defines the computational domain size $L_d = M \lambda_c$ as M -multiple of the characteristic wavelength λ_c , and $\gamma = \frac{U}{a}$

249	represents the factor to normalize the total energy in the state	311
250	variable u_Λ to one.	312
251	Is there a difference between L_0 and L_d? typo?	313
252	Consider the spatial discretization $J = 2\Lambda + 1$ so that the	314
253	smallest resolved scale is comparable with the characteristic	315
254	wavelength	316
255		317
256	$\Delta x = \frac{2\pi M \lambda_c}{J} \lesssim \lambda_c \Rightarrow M = \frac{J}{2\pi} \sim 5, J = 32.$	318
257		319
258	Therefore in the practical numerical simulations, we pick	320
259	$M = 5$ and γ varies in the range $[0.5, 1]$. Using the reference	321
260	experimental measurements (20), $\epsilon \in [0.0024, 0.024]$, $\delta \sim 0.22$,	322
261	and D_0 changes from 1 to 0.24 before and after the depth	323
262	change. The reference values for the model scales can be es-	324
263	timated in the range $L_0 \in [2, 6]$ and $E_0 \in [50, 200]$. These are	325
264	the values we will test in the direct numerical simulations. See	326
265	details about the derivation from scale analysis in <i>SI Appendix,</i>	327
266	A .	328
267		329
268	3. Equilibrium statistical mechanism for generating	330
269	the stationary invariant measure	331
270		332
271	In this section title, did you mean ‘statistical mechanism’ or	333
272	‘statistical mechanics’?	334
273		335
274	Since the TKdV equation satisfies the Liouville property,	336
275	the equilibrium invariant measure can be described by an equi-	337
276	librium statistical formulism (22–24) using a Gibbs measure	338
277	with the conserved energy \mathcal{E}_Λ and Hamiltonian \mathcal{H}_Λ . The equi-	339
278	librium invariant measure is dictated by the conservation laws	340
279	in the TKdV equation. In the case with fixed total energy E_0 ,	341
280	this is the <i>mixed Gibbs measure</i> in the truncated model with	342
281	microcanonical energy and canonical Hamiltonian ensembles	343
282	(22)	344
283	$\mathcal{G}_\theta^\pm(u_\Lambda^\pm; E_0) = C_\theta^\pm \exp(-\theta^\pm \mathcal{H}(u_\Lambda^\pm)) \delta(\mathcal{E}(u_\Lambda^\pm) - E_0), \quad [3]$	345
284		346
285	with θ representing the “inverse temperature”. The distinct	347
286	statistics in the upstream and downstream waves can be con-	348
287	trolled by the value of θ . Negative temperature, $\theta^\pm < 0$, is	349
288	the appropriate regime to predict the experiments as shown	350
289	below. In the incoming flow field, the inverse temperature θ^-	351
290	is chosen so that \mathcal{G}_θ^- has Gaussian statistics. Using the above	352
291	invariant measures [3], the expectation of any functional $F(u)$	353
292	can be computed based on the Gibbs measure	354
293		355
294	$\langle F \rangle_{\mathcal{G}_\theta} \equiv \int F(u) \mathcal{G}_\theta(u) du.$	356
295		357
296		358
297	The value of θ in the invariant measure is specified from $\langle H_\Lambda \rangle_{\mathcal{G}_\theta}$	359
298	(22, 24). The invariant measure also predicts an equilibrium	360
299	energy spectrum without running the TKdV equation directly.	361
300	On the other hand, the time autocorrelation and transient	362
301	statistics about the state variable u_Λ cannot be recovered from	363
302	the statistical theory.	364
303		365
304	Statistical matching condition in invariant measures before	366
305	and after the abrupt depth change. The Gibbs measures \mathcal{G}_θ^\pm	367
306	are defined based on the different inverse temperatures θ^\pm on	368
307	the two sides of the solutions	369
308	$\mu_t^-(u_\Lambda^-; D_-), \quad u_\Lambda _{t=T_{\text{ADC}}^-} = u_0, \quad t < T_{\text{ADC}};$	370
309	$\mu_t^+(u_\Lambda^+; D_+), \quad u_\Lambda _{t=T_{\text{ADC}}^+} = u_0, \quad t > T_{\text{ADC}},$	371
310		372

373 property as measured by the decay of autocorrelations as long
 374 as the system starts from a negative inverse temperature state
 375 as described before. For direct numerical simulations of the
 376 TKdV equations, a proper symplectic integrator is required to
 377 guarantee the Hamiltonian and energy are conserved in time.
 378 It is crucial to use the symplectic scheme to guarantee the
 379 exact conservation of the energy and Hamiltonian since they
 380 are playing the central role in generating the invariant measure
 381 and the statistical matching. The symplectic schemes used
 382 here for the time integration of the equation is the 4th-order
 383 midpoint method (25). Details about the mixing properties
 384 from different initial states and the numerical algorithm are
 385 described in *SI Appendix, C*.



417 **Fig. 1.** First row: skewness from the Gibbs measures in incoming and outgoing flow
 418 states with different values of total energy E_0 and inverse temperature θ (notice
 419 the different scales in the incoming and outgoing flows); Second row:
 420 outgoing flow parameter θ^+ as a function of the incoming flow θ^- computed from the statistical
 421 matching condition with three energy level E_0 ; Last row: skewness in the outgoing
 422 flow with the matched value of θ^+ as a function of the inflow parameter θ^- (the
 423 theoretical predictions using [5] are compared).

425 5. Predicting extreme anomalous behavior after the 426 ADC by statistical matching

427 With the inflow statistics well described and the numerical
 428 scheme set up, we are able to predict the downstream anomalous
 429 statistics starting from the near-Gaussian incoming flow
 430 going through the abrupt depth change from $D_- = 1$ to
 431 $D_+ = 0.24$. First, we consider the statistical prediction in the
 432 downstream equilibrium measure directly from the matching
 433 condition. The downstream parameter value θ^+ is determined
 434

435 by solving the nonlinear equation [4] as a function of θ^+ ,
 436 $F(\theta^+) = \langle H_\Lambda^+ \rangle_{\mathcal{G}_\theta^+}(\theta^+) - \langle H_\Lambda^+ \rangle_{\mathcal{G}_\theta^-} = 0$. In the numerical
 437 approach, we adopt a modified secant method avoiding the
 438 stiffness in the parameter regime (see the *SI Appendix, B.2*
 439 for the algorithm). The fitted solution is plotted in Figure
 440 1 (b) as a function of the proposed inflow θ^- . A nonlinear
 441 θ^- - θ^+ relation is discovered from the matching condition. The
 442 downstream inverse temperature θ^+ will finally saturate at
 443 some level. The corresponding downstream skewness of the
 444 wave displacement u_Λ predicted from the statistical matching
 445 of Gibbs measures is plotted in Figure 1 (c). In general, a
 446 large positive skewness for outgoing flow κ_3^+ is predicted from
 447 the theory, while the incoming flow skewness κ_3^- is kept in
 448 a small value in a wide range of θ^- . Note that with $\theta^- \sim 0$
 449 (that is, using the microcanonical ensemble only with energy
 450 conservation), the outflow statistics are also near Gaussian
 451 with weak skewness. The skewness in the outflow statistics
 452 grows as the inflow parameter value θ^- increases in amplitude.
 453

454 For a second approach, we can use direct numerical simulations
 455 starting from the initial state sampled from the incoming
 456 flow Gibbs measure \mathcal{G}_θ^- and check the transient changes in the
 457 model statistics. Figure 2 illustrates the change of statistics
 458 as the flow goes through the abrupt depth change. The first
 459 row plots the changes in the skewness and kurtosis for the
 460 state variable u_Λ after the depth change at $t = 0$. The PDFs
 461 in the incoming and outgoing flow states are compared with
 462 three different initial inverse temperatures θ^- . After the depth
 463 changes to $D_0 = 0.24$ abruptly at $t = 0$, both the skewness
 464 and kurtosis jump to a much larger value in a short time,
 465 implying the rapid transition to a highly skewed non-Gaussian
 466 statistical regime after the depth change. Further from Figure
 467 2, different initial skewness (but all relatively small) is set
 468 due to the various values of θ^- . With small $\theta^- = -0.1$, the
 469 change in the skewness is not very obvious (see the second row
 470 of Figure 2 for the incoming and outgoing PDFs of u_Λ). In
 471 comparison, if the incoming flow starts from the initial param-
 472 eter $\theta^- = -0.3$ and $\theta^- = -0.5$, much larger increase in the
 473 skewness is induced from the abrupt depth change. Further-
 474 more, in the detailed plots in the third row of Figure 2 for the
 475 downstream PDFs under logarithmic scale, fat tails towards
 476 the positive direction can be observed, which represent the
 477 extreme events in the downstream flow (see also Figure 3 for
 478 the time-series of u_Λ).

479 As a result, the downstream statistics in final equilibrium
 480 predicted from the direct numerical simulations here agree with
 481 the equilibrium statistical mechanism prediction illustrated in
 482 Figure 1. The prediction from these two different approaches
 483 confirm each other.

484 Again, do we mean statistical ‘mechanism’ or ‘mechanics’?

485 6. Analytic formula for the upstream skewness after 486 the ADC

487 A statistical link between the upstream and downstream en-
 488 ergy spectra can be found for an analytical prediction of the
 489 skewness in the flow state u after the ADC. The skewness of
 490 the state variable u_j at one spatial grid point is defined as the
 491 ratio between the third and second moments
 492

$$\kappa_3 = \langle u_j^3 \rangle_\mu / \langle u_j^2 \rangle_\mu^{3/2}.$$

497
498
499
500
501
502
503
504
505
506
507
508
509
510
511
512
513
514
515
516
517
518
519

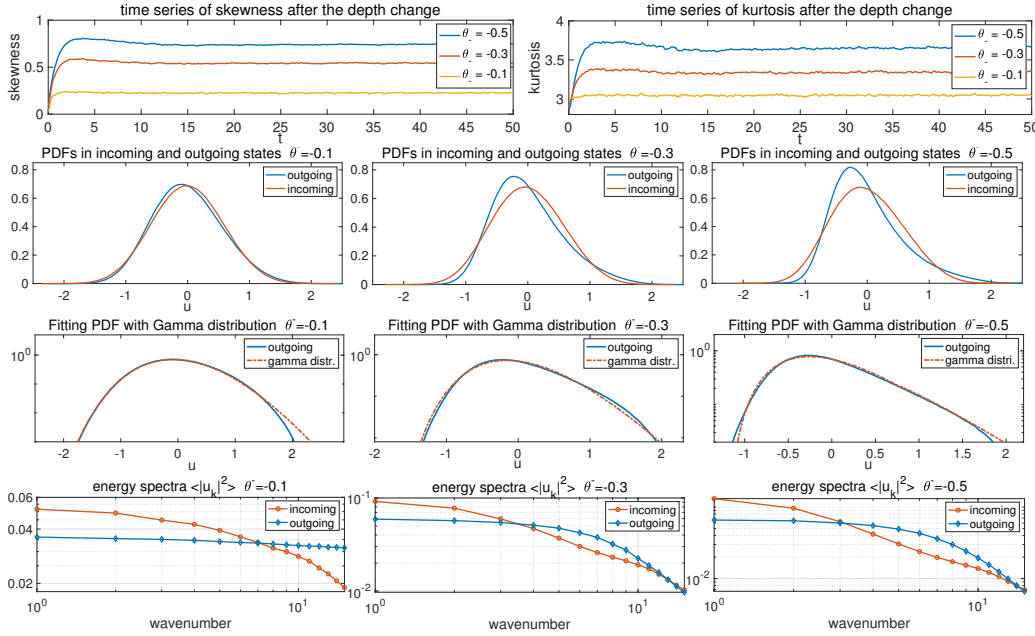


Fig. 2. Changes in the statistics of the flow state going through the abrupt depth change. The initial ensemble is set with the incoming flow Gibbs measure with different inverse temperature θ^- . First row: time evolution of the skewness and kurtosis. The abrupt depth change is taking place at $t = 0$; Second row: inflow and outflow PDFs of u_Λ ; Third row: the downstream PDFs fitted with Gamma distributions with consistent variance and skewness (in log coordinate in y); Last row: energy spectra in the incoming and outgoing flows.

523

524 Now we introduce mild assumptions on the distribution functions:

- 527 • The upstream equilibrium measure μ_- has a relatively 528 small skewness so that

$$530 \quad \langle H_3 \rangle_{\mu_-} = \frac{1}{6} \int_{-\pi}^{\pi} \langle u^3 \rangle_{\mu_-} dx \equiv \epsilon;$$

- 533 • The downstream equilibrium measure μ_+ is homogeneous 534 at each physical grid point, so that the second and third 535 moments are invariant at each grid point

$$536 \quad \langle u_j^2 \rangle_{\mu_+} = \sigma^2 = \pi^{-1}, \quad \langle u_j^3 \rangle_{\mu_+} = \sigma^3 \kappa_3 = \pi^{-\frac{3}{2}} \kappa_3^+.$$

538 Then the skewness of the downstream state variable u_Λ^+ after 539 the ADC is given by the difference between the inflow and 540 outflow wave slope energy of u_x

$$543 \quad \kappa_3^+ = \frac{3}{2} \pi^{\frac{1}{2}} L_0^{-\frac{3}{2}} E_0^{-\frac{1}{2}} D_+^2 \int_{-\pi}^{\pi} \left[\langle u_x^2 \rangle_{\mu_+} - \langle u_x^2 \rangle_{\mu_-} \right] dx + 3\pi^{\frac{1}{2}} \epsilon. \quad [5]$$

546 The detailed derivation is shown in [SI Appendix, B.2](#). In 547 particular, the downstream skewness with near-Gaussian inflow 548 statistics $\epsilon \ll 1$ is positive if and only if the difference of the 549 incoming and outgoing wave slope energy is positive. This 550 means that there is more small scale wave slope energy in the 551 outgoing state. As an evidence, in the last row of Figure 2 552 in all the weak and strong skewness cases, the outflow energy 553 spectrum always has a slower decay rate than the inflow energy 554 spectrum which possesses stronger energy in larger scales and 555 weaker energy in the smaller scales.

557 In Figure 1 (c), we compare the accuracy of the theoretical 558 estimation [5] with numerical tests. In the regime with small

559 incoming inverse temperature θ^- , the theoretical formula offers 560 a quite accurate approximation of the third-order skewness 561 using only information from the second-order moments of the 562 wave-slope spectrum.

7. Key features from experiments captured by the statistical dynamical model

In this final section, we emphasize the crucial features generated by the statistical dynamical model [1] by making comparison with the experimental observations in (20). As from the scale analysis displayed in Section 2, the theory is set in the same parameter regime as the experimental setup.

- 600 • The transition from near-Gaussian to skewed non-Gaussian distribution as well as the jump in both skewness 601 and kurtosis observed in the experiment observations (Fig. 602 1 of (20)) can be characterized by the statistical model 603 simulation results (see the first and second row of Figure 604 2). Notice that the difference in the decay of third and 605 fourth moments in the far end of the downstream regime 606 from the experimental data is due to the dissipation effect 607 in the flow from the wave absorbers that is not modeled 608 in the statistical model here. The model simulation 609 time-series plotted in Figure 3 can be compared with 610 the observed time sequences from experiments (Fig. 1 of 611 (20)). The downstream simulation generates waves with 612 strong and frequent intermittency towards the positive 613 displacement, while the upstream waves show symmetric 614 displacements in two directions with at most small peaks 615 in slow time. Even in the time-series at a single location 616 $x = 0$, the long-time variation displays similar structures.
- 617 • The downstream PDFs in experimental data are estimated 618 with a Gamma distribution in Fig. 2 of (20). Here in 619

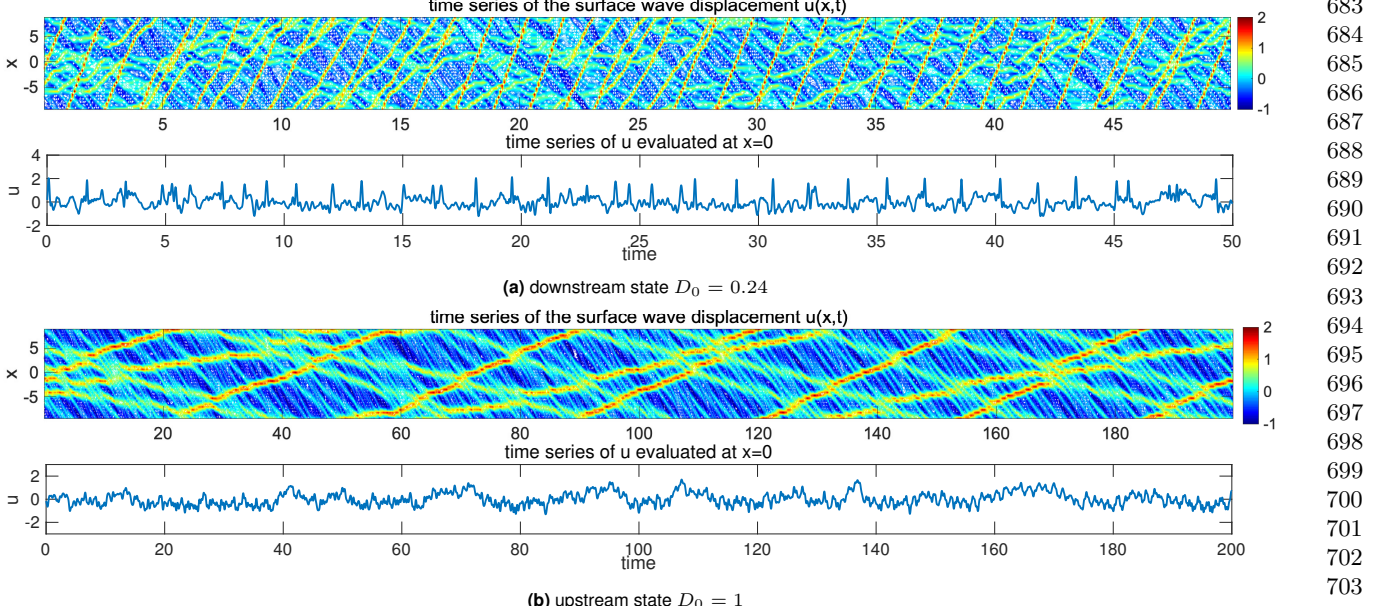


Fig. 3. Realization of the downstream and upstream flow solutions u_A^\pm . Note the larger vertical scale in the downstream time-series plot.

I do not understand the last sentence above. Why does the peak frequency illustrate the occurrence of transporting water waves?

the same way, we can fit the highly skewed outgoing flow PDFs from the numerical results with the Gamma distribution

$$\rho(u; k, \alpha) = \frac{e^{-k} \alpha^{-1}}{\Gamma(k)} (k + \alpha^{-1} u)^{k-1} e^{-\alpha^{-1} u}.$$

The parameters (k, α) in the Gamma distribution are fitted according to the measured statistics in skewness and variance, that is, $\sigma^2 = k\alpha^2$, $\kappa_3 = 2/\sqrt{k}$. And the excess kurtosis of the Gamma distribution can be recovered as $\kappa_4 = 6/k$. As shown in the third row of Figure 2, excellent agreement in the PDFs with the Gamma distributions is reached in consistency with the experimental data observations. The accuracy with this approximation increases as the initial inverse temperature θ^- increases in value to generate more skewed distribution functions.

- The experiments also have the up and down stream power spectra in time (Fig. 4 of (20)), which shows more energy at small time scales, i.e., a relatively slower decay rate in the downstream compared with the upstream case. This is also observed in the direct numerical simulations here (detailed results shown in *SI Appendix, C.2*). The downstream state contains more energetic high frequencies. The peak frequency illustrates the occurrence of the transporting waves along the water tank.

8. Concluding discussion

We have developed a statistical dynamical model to explain and predict extreme events and anomalous features of shallow water waves crossing an abrupt depth change. The theory is based on the dynamical modeling strategy consisting of the TKdV equation matched at the abrupt depth change with conservation of energy and Hamiltonian. Predictions can be made of the extreme events and anomalous features by matching incoming and outgoing statistical Gibbs measures before and after the abrupt depth transition. The statistical matching of the known nearly Gaussian incoming Gibbs state completely determines the predicted anomalous outgoing Gibbs state, which can be calculated by a simple sampling algorithm, verified by direct numerical simulations, and successfully captures key features of the experiment. An analytic formula for the anomalous outgoing skewness is also derived. The strategy here should be useful for predicting extreme statistical events in other dispersive media in different settings.

ACKNOWLEDGMENTS. This research of A. J. M. is partially supported by the Office of Naval Research through MURI N00014-16-1-2161. D. Q. is supported as a postdoctoral fellow on the second grant. M.N.J.M would like to acknowledge support from Simons grant 524259.

1. Majda AJ, Branicki M (2012) Lessons in uncertainty quantification for turbulent dynamical systems. *Discrete & Continuous Dynamical Systems-A* 32(9):3133–3221.
2. Mohamad MA, Sapsis TP (2018) A sequential sampling strategy for extreme event statistics in nonlinear dynamical systems. *Proceedings of the National Academy of Sciences* 115(44):11138–11143.
3. Qi D, Majda AJ (2016) Predicting fat-tailed intermittent probability distributions in passive scalar turbulence with imperfect models through empirical information theory. *Communications in Mathematical Sciences* 14(6):1687–1722.
4. Majda AJ, Tong XT (2015) Intermittency in turbulent diffusion models with a mean gradient. *Nonlinearity* 28(11):4171–4208.
5. Majda AJ, Chen N (2018) Model error, information barriers, state estimation and prediction in complex multiscale systems. *Entropy* 20(9):644.
6. Majda AJ, Tong XT (2018) Simple nonlinear models with rigorous extreme events and heavy tails. <https://www.pnas.org/doi/10.1073/pnas.XXXXXXXXXX>
7. Thual S, Majda AJ, Chen N, Stechmann SN (2016) Simple stochastic model for el nino with westerly wind bursts. *Proceedings of the National Academy of Sciences* 113(37):10245–10250.
8. Chen N, Majda AJ (2018) Efficient statistically accurate algorithms for the Fokker-Planck
13. Cousins W, Sapsis TP (2015) Unsteady evolution of localized unidirectional deep-water wave groups. *Physical Review E* 91(6):063204.
14. Farazmand M, Sapsis TP (2017) Reduced-order prediction of rogue waves in two-dimensional deep-water waves. *Journal of Computational Physics* 340:418–434.
15. Onorato M, Osborne AR, Serio M, Bertone S (2001) Freak waves in random oceanic sea states. *Physical Review Letters* 86(25):5831–5834.
16. Dematteis G, Grafke T, Vanden-Eijnden E (2018) Rogue waves and large deviations in deep sea. *Proceedings of the National Academy of Sciences* 115(5):855–860.
17. Sergeeva A, Pelinovsky E, Talipova T (2011) Nonlinear random wave field in shallow water: variable Korteweg-de Vries framework. *Natural Hazards and Earth System Sciences* 11(2):323–330.
18. Trulsen K, Zeng H, Gramstad O (2012) Laboratory evidence of freak waves provoked by non-uniform bathymetry. *Physics of Fluids* 24(9):097101.
19. Viotti C, Dias F (2014) Extreme waves induced by strong depth transitions: Majda et al. results. *Physics of Fluids* 26(5):051705.
20. Bolles CT, Speer K, Moore MNJ (2018) Anomalous wave statistics induced by abrupt depth change. *arXiv preprint arXiv:1808.07958*.
21. Johnson RS (1997) *A modern introduction to the mathematical theory of water waves*. (Cambridge University Press, Cambridge)